Ahmed H. El-Shaer
Hitachi Global Storage Technologies (HGST),
San Jose, CA 95119
e-mail: aheshaer@gmail.com

Mohammad Al Janaideh[1]
Department of Mechatronics Engineering,
The University of Jordan,
Amman 11942, Jordan
e-mail: aljanaideh@gmail.com

Pavel Krejčí
Mathematical Institute,
Academy of Sciences of the Czech Republic,
Žitná 25,
CZ-11567 Praha 1, Czech Republic
e-mail: krejci@math.cas.cz

Masayoshi Tomizuka
Department of Mechanical Engineering,
University of California,
Berkeley, CA 94720
e-mail: tomizuka@me.berkeley.edu

Robust Performance Enhancement Using Disturbance Observers for Hysteresis Compensation Based on Generalized Prandtl–Ishlinskii Model

This paper presents an approach employing disturbance observers to enhance the performance of inverse-based hysteresis compensation based on the generalized Prandtl–Ishlinskii model in feedback control reference-tracking applications. It is first shown that the error resulting from inexact hysteresis compensation is an L_∞-bounded signal. Hence, a disturbance observer (DOB) is designed to cancel its effect and improve the closed loop robust tracking performance in the presence of plant dynamics uncertainty. The design of the DOB makes use of an equivalent internal model-based estimation of exogenous disturbances, where the internal model dynamics is designed to have at least an eigenvalue at the origin. The synthesis is then formulated as an H_∞ weighted-sensitivity optimization for static output feedback (SOF) gain of a Luenberger observer. A linearization heuristic is then implemented to solve the bilinear-matrix-inequality (BMI) constrained semidefinite program (SDP) for a (sub)optimal static gain. Simulation results indicate that tracking performance is indeed improved using the combined inversion-based compensation and the DOB. [DOI: 10.1115/1.4023762]

1 Introduction

Smart material-based actuators exhibit strong hysteresis nonlinearities, causing performance degradation and potential instability of their closed-loop systems [1]. Lately, a variety of control methods have been developed in the literature for compensation of hysteresis nonlinearities (see Refs. [1–13]). The majority of such techniques can be classified as inverse-based, and noninverse-based compensation. In the inverse-based approach, an "estimated" inverse of the hysteresis is employed to compensate its effect. On the other hand, noninverse compensation regards the hysteresis nonlinearity as a disturbance modeled by a given operator-based hysteresis model [14]. This, however, can be valid for a number of hysteretic actuators operated at low frequencies in well-known excitation conditions (e.g. temperature, mechanical, stress level, etc.). Nevertheless, different experimental studies show that hysteresis effects are not "simple" nonlinearities to be considered as disturbances [15]. Thus, to effectively compensate hysteresis effects operating at different excitation frequencies and eliminate potential limit cycles resulting from inexact compensation, it is essential to employ an inverse-based compensation of the hysteresis.

A generalized Prandtl–Ishlinskii model and its inverse have been presented to characterize and compensate for hysteresis nonlinearities [16,17]. This model extends the classic operator-based Prandtl–Ishlinskii model to describe symmetric as well as asymmetric and saturated hysteresis loops. Unlike the Preisach and Krasnosel'skii–Pokrovskii models, the generalized Prandtl–Ishlinskii model has the uniquely attractive property of being analytically invertible. This analytic invertibility of the generalized Prandtl–Ishlinskii model may serve as an effective means for inverse-based hysteresis compensation utilizing feedforward compensators (see Ref. [18] for details).

The work in this paper focuses on closed-loop robust tracking performance for SISO feedback systems employing inverse model-based hysteresis compensation. In this setting, the nominal plant is assumed to be a linear time-invariant (LTI) system preceded by the hysteresis nonlinearity. A compensator applying the inverse generalized Prandtl–Ishlinskii model is used to compensate the hysteretic effects. Nevertheless, model mismatch between the hysteresis nonlinearity and the estimate of its inverse often leads to inexact compensation. Thus, to account for inaccuracies due variations in the operating conditions, uncertainty in the actuator dynamics and exogenous disturbances, a disturbance observer (DOB) is used. In DOB-based control, an inner loop employing unity-DC gain low pass filter $Q(s)$ is added into the main feedback system to estimate input disturbances and cancel them subsequently [19–23].

The DOB synthesis in this paper relies on the equivalence of DOB structure shown in Fig. 3 and that of state estimation of an augmented state space system utilizing an internal model for the exogenous disturbance with at least one eigenvalue at the origin (see Theorem 1). The equivalence between classic internal model approach [24] and the DOB structure is shown in [21]. However, a design procedure for an optimal DOB is not given there. Thus, using the latter approach, DOB synthesis is formulated as an H_∞ weighted sensitivity optimization of a static output feedback (SOF) gain of a Luenberger observer. This is appealing for the following reasons: (i) the design of the outer loop controller achieving nominal tracking performance, and the DOB inner loop can be carried out separately. Specifically, robust disturbance rejection is optimized in the presence of a given outer controller which ensure robust performance of the overall closed-loop system. (ii) The DOB filter $Q(s)$ having unity dc-gain can be designed with more flexibility in regards to its order, bandwidth, and roll-off rate, which greatly enhances disturbance rejection performance and robustness of the overall system. Also, having unity dc-gain over wide enough bandwidth, disturbance rejection could be achieved

[1]Corresponding author.

Contributed by the Dynamic Systems Division of ASME for publication in the Journal of Dynamic Systems, Measurement and Control. Manuscript received December 20, 2011; final manuscript received December 17, 2012; published online May 29, 2013. Assoc. Editor: Sergey Nersesov.

for a large class of disturbance signals without precise knowledge of the disturbance model as long as the frequency content lies within the DOB bandwidth. This simple fact is central to the development of robust disturbance rejection in the sequel since it is not straight forward to construct an accurate signal model for the hysteresis compensation error in feedback applications. (iii) The synthesis optimization is cast as semidefinite programming (SDP) which can be solved very efficiently using reliable and readily available software [25]. This offers a great advantage over the Riccati equation-based solution to H_∞ optimization which fails to exist in the presence of uncontrollable and/or unobservable $j\omega$-axis poles present in internal model-based synthesis [26].

The main contributions of this paper are: (1) L_∞-boundedness for inverse-based hysteresis compensation error is analytically demonstrated for a generalized Prandtl–Ishlinskii model, which in turn is treated as a bounded exogenous disturbance whose effect can be rejected using the DOB; (2) hysteresis compensation is systematically treated using powerful tools from robust control theory, building upon results of the H_∞ framework to guarantee closed-loop robust performance [8,27]; (3) the design of the DOB filter $Q(s)$ is reduced to an SOF controller which has a simpler structure than that of $Q(s)$ in conventional DOB work. The design framework developed in this paper makes fairly nonrestrictive assumptions on the plant characteristics. Furthermore, a number of robust state estimation/disturbance rejection approaches studied in the literature can be systematically recovered using the DOB design approach in this paper. This can be done by choosing appropriate internal model dynamics for the exogenous disturbances [28].

The paper is organized as follows. In Sec. 2, a generalized Prandtl–Ishlinskii model with its inverse are given. This section also derives a bound on inexact hysteresis compensation. Section 3 discusses the closed-loop DOB-based hysteresis error compensation to be investigated. An overview of DOBs and their relation to internal model-based state estimation is developed in Sec. 4. A synthesis approach utilizing SDP optimization is then presented. Section 5 is devoted to optimization synthesis results and closed-loop simulation of a number of hysteresis compensation scenarios.

2 A Generalized Prandtl–Ishlinskii Model and its Inverse

In this section, the generalized Prandtl–Ishlinskii model and its inverse are presented. This model has been used for different hysteresis nonlinearities in smart actuators [14,17]. It is proved that the error resulting from inexact feedforward inverse-based compensation of the generalized Prandtl–Ishlinskii model is an L_∞-bounded signal.

2.1 Generalized Prandtl–Ishlinskii Model. For a given input $v(t) \in C[0,T]$ (i.e. continuous function), the output $w(t)$ of the generalized Prandtl–Ishlinskii model can be expressed as $w(t) = H[v](t) = G[\delta(v)](t)$, where G is the Prandtl–Ishlinskii model given by the Stieltjes integral

$$G[u](t) = p(0)u(t) + \int_0^\infty F_r[u](t)dp(r) = -\int_0^\infty \frac{\partial}{\partial r}(F_r[u](t))p(r)dr \tag{1}$$

where $p(r)$ is a nondecreasing left-continuous density function, $F_r[u](t)$ is output of the play operator with threshold $r>0$ and input $u(t) = \delta(v(t))$. The function $\delta : \mathbb{R} \to \mathbb{R}$ is an envelope function which, together with its inverse $\delta^{-1} : \mathbb{R} \to \mathbb{R}$, is strictly increasing, continuous and odd. Here, it is also assumed that both δ and δ^{-1} are Lipschitz continuous. The integration by parts in Eq. (1) holds under the convention $F_0[u](t) = u(t)$, which is compatible with Eq. (2). It is recalled that the output of each individual play operator F_{r_j} is defined for monotone (nondecreasing or nonincreasing) functions u in each interval $[t_{i-1}, t_i]$ of a partition $0 = t_0 < \cdots < t_m = T$ by

$$F_{r_j}[u](t) = \max(v(t) - r_j, \min(u(t) + r_j, F_{r_j}[u](t_{i-1}))) \tag{2}$$

for $t \in [t_{i-1}, t_i]$, with initial condition $F_{r_j}[u](0) = \max(u(0) - r_j, \min(u(0) + r_j, 0))$ corresponding to no initial memory. The definition can be extended to the whole space $C[0, T]$ by density argument as in Ref. [7]. If $p(r)$ is a piecewise constant step function of the form

$$p(r) = \sum_{j=0}^{l} p_j, \quad r \in [r_l, r_{l+1}), \quad l = 0, \ldots, N \tag{3}$$

where $0 = r_0 \le r_1 \cdots \le r_N \le r_{N+1} = \infty$ is a given sequence of thresholds and p_j are constant positive weights, then the Prandtl–Ishlinskii model can be expressed as

$$G[u](t) = \sum_{j=0}^{N} p_j F_{r_j}[u](t) = p_0 u(t) + \sum_{j=1}^{N} p_j F_{r_j}[u](t) \tag{4}$$

which is the classical discrete Prandtl–Ishlinskii model. For the identity envelope function $\delta(v) = v$, the generalized Prandtl–Ishlinskii model H reduces to the classical Prandtl–Ishlinskii model presented in Ref. [7]. Lipschitz-continuity of the generalized Prandtl–Ishlinskii model is ensured since the function δ is itself Lipschitz-continuous.

2.2 Inverse Generalized Prandtl–Ishlinskii Model. The reported studies involving inverse compensation generally exhibit compensation errors, even when the exact inverse is employed. This error has been attributed to the characterization errors of the generalized Prandtl–Ishlinskii model. The resulting model generally exhibits some degree of error between the model output and the measured characteristics. The estimated hysteresis models have been employed to construct the inverse of the Preisach, Krasnosel'skii–Pokrovskii and Prandtl–Ishlinskii models [29].

Indeed, the exact inverse operator $v = H^{-1}[w]$ to $w = H[v] = G[\delta(v)]$ can be written in the form

$$H^{-1}[w](t) = \delta^{-1}(G^{-1}[w](t)) \tag{5}$$

where $\delta^{-1} : \mathbb{R} \to \mathbb{R}$ is the inverse of δ, and G^{-1} is the inverse Prandtl–Ishlinskii operator of G given by Ref. [7]

$$G^{-1}[w](t) = g_0 w(t) + \sum_{j=1}^{N} g_j F_{s_j}[w](t) \tag{6}$$

The weights g_j and thresholds s_j, $j = 0, \ldots, N$, of the exact inverse G^{-1}, putting $r_0 = s_0 = 0$, can be written as [7]

$$s_j - s_{j-1} = \sum_{i=0}^{j-1} p_i (r_j - r_{j-1}) \tag{7}$$

$$g_0 = \frac{1}{p_0}, \quad g_j = -\frac{p_j}{\left(p_0 + \sum_{i=1}^{j} p_i\right)\left(p_0 + \sum_{i=1}^{j-1} p_i\right)} \tag{8}$$

It is assumed that the function δ^{-1} and the weights g_j and thresholds s_j of the inverse G^{-1} are not exactly known, but only their approximations $\hat{\delta}^{-1}$, $\hat{g}_j$, and $\hat{s}_j$ are available. We propose an estimated inverse generalized Prandtl–Ishlinskii model in the form

$$\hat{H}^{-1}[w](t) = \hat{\delta}^{-1}(\hat{G}^{-1}[w](t)) \tag{9}$$

where

$$\hat{G}^{-1}[w](t) = \hat{g}_0 w(t) + \sum_{j=1}^{M} \hat{g}_j F_{\hat{s}_j}[w](t) \tag{10}$$

and find an upper bound for the compensation error. In practical applications, it will be convenient to take $M < N$ in order to reduce the computational complexity.

2.3 Error of the Inverse Compensation. In this subsection, we estimate the error of the inverse compensation when the approximate generalized Prandtl–Ishlinskii model is applied to compensate for the hysteresis in the generalized Prandtl–Ishlinskii model. We first introduce the functions ϕ and $\hat{\phi}$

$$\phi(s) = \sum_{k=0}^{j} g_k, \quad s \in [s_j, s_{j+1}), \quad j = 0, \ldots, N \tag{11}$$

$$\hat{\phi}(s) = \sum_{k=0}^{j} \hat{g}_k, \quad s \in [\hat{s}_j, \hat{s}_{j+1}), \quad j = 0, \ldots, M \tag{12}$$

again with $s_{N+1} = \hat{s}_{M+1} = \infty$. It is convenient to rewrite the identities in Eq. (6) and (10), using the integration by parts formula, in terms of integrals analogous to Eq. (1)

$$\begin{aligned} G^{-1}[w](t) &= \phi(0)w(t) + \int_0^\infty F_s[w](t)d\phi(s) \\ &= -\int_0^\infty \frac{\partial}{\partial s}(F_s[w](t))\phi(s)ds \end{aligned} \tag{13}$$

$$\begin{aligned} \hat{G}^{-1}[w](t) &= \hat{\phi}(0)w(t) + \int_0^\infty F_s[w](t)d\hat{\phi}(s) \\ &= -\int_0^\infty \frac{\partial}{\partial s}(F_s[w](t))\hat{\phi}(s)ds \end{aligned} \tag{14}$$

Hence, $F_s[w](t) = 0$ for $s > ||w||_\infty := \sup_t w(t)$, and $|(\partial/\partial s) F_s[w](t)| \leq 1$ almost everywhere. It follows that

$$|\hat{G}^{-1}[w](t) - G^{-1}[w](t)| \leq \int_0^{||w||_\infty} |\hat{\phi}(s) - \phi(s)|ds \tag{15}$$

Let $v(t)$ be an input signal and $w(t) = G[\delta(v)](t)$ be the output. The approximate inversion error between $v(t)$ and $\hat{v}(t) = \hat{\delta}^{-1}(\hat{G}^{-1}[w](t))$ can be estimated as follows

$$\begin{aligned} ||v - \hat{v}||_\infty &= ||\delta^{-1}(G^{-1}[w]) - \hat{\delta}^{-1}(\hat{G}^{-1}[w])||_\infty \\ &\leq ||\delta^{-1}(\hat{G}^{-1}[w]) - \hat{\delta}^{-1}(\hat{G}^{-1}[w])||_\infty \\ &\quad + ||\delta^{-1}(G^{-1}[w]) - \delta^{-1}(\hat{G}^{-1}[w])||_\infty \\ &\leq ||\delta^{-1} - \hat{\delta}^{-1}||_\infty + L_\delta \int_0^{||w||_\infty} |\hat{\phi}(s) - \phi(s)|ds \end{aligned} \tag{16}$$

where L_δ is the Lipschitz constant of δ^{-1}.

3 Problem Statement: Inversion-Based Hysteresis Compensation With DOBs

This paper is concerned with improving the performance of inversion-based hysteresis compensation using disturbance observers (DOBs). Shown in Fig. 1 is the inversion-based hysteresis compensation without DOB. The plant is comprised of a stable SISO LTI system $P(s)$ and the hysteresis nonlinearity $H(.)$ whose output is denoted by $\eta(t)$. Moreover, the feedback controller is

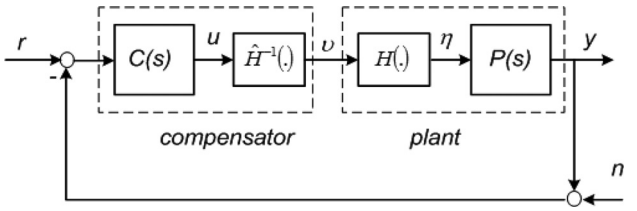

Fig. 1 Inversion-based hysteresis compensation scheme without DOB

composed of an internally stabilizing SISO LTI system and a nonlinearity $\hat{H}^{-1}(.)$ giving an estimate of the inverse of $H(.)$. In Fig. 1, the signals $r(t)$ and $n(t)$ are reference input and measurement noise, respectively.

The presence of model uncertainty and variation in operating conditions result in inexact hysteresis compensation, and the difference $\eta(t) - u(t)$ will not necessarily vanish. More specifically, we have [29–31]

$$\eta(t) = H\big(\hat{H}^{-1}[u]\big)(t) = u(t) + \delta_H(t, u(t)) \ \forall t \geq 0 \tag{17}$$

where $u(t)$ is the nominal control input and $\delta_H : \mathbb{R}_+ \times \mathbb{R} \to \mathbb{R}$ is a time varying nonlinearity representing the compensation error. By hypothesis, the operator H is Lipschitz continuous in $C[0, T]$, and it follows from Eq. (16) that $\delta_H \in L_\infty$.

In addition to hysteresis compensation error, the more general case of having a bounded exogenous disturbance d_{ex} at the plant input is now considered; $\eta(t) = H\big(\hat{H}^{-1}[u] + d_{ex}\big)(t)$. Suppose that $L_H > 0$ is the Lipschitz constant of H, it follows that

$$\begin{aligned} &\big|H\big(\hat{H}^{-1}[u] + d_{ex}\big)(t) - H\big(\hat{H}^{-1}[u]\big)(t)\big| \leq L_H|d_{ex}(t)| \\ &\Rightarrow \big|H\big(\hat{H}^{-1}[u] + d_{ex}\big)(t)\big| \leq L_H|d_{ex}(t)| + |u(t) + \delta_H(t, u(t))| \end{aligned} \tag{18}$$

where Eq. (17) is substituted for $H\big(\hat{H}^{-1}[u]\big)$. The output $y(t)$ in the presence of d_{ex} can be written as

$$y(t) = \int_0^t g(t-\tau) \underbrace{H\big(\hat{H}^{-1}[u] + d_{ex}\big)(\tau)}_{\eta(\tau)} d\tau \quad \forall t \geq 0 \tag{19}$$

where $g(t)$ is the impulse response of the stable LTI system $P(s)$. From Eq. (18), it follows that

$$\sup_{t\geq 0} |y(t)| \leq ||g||_{L_1} \Big(L_H ||d_{ex}||_\infty + \sup_{t\geq 0} |u(t) + \delta_H(t, u(t))| \Big) \tag{20}$$

where $||g||_{L_1} := \int_0^\infty |g(t)|dt$. The righthand side of Eq. (20) is finite if and only if the transfer functions $\begin{bmatrix} 1 & P(s) \\ -C(s) & 1 \end{bmatrix}^{-1}$ are asymptotically (exponentially) stable [8], which together with Eq. (16) guarantees that $\sup_{t\geq 0} |u(t) + \delta_H(t, u(t))|$ is uniformly bounded.

Henceforth, $d(t)$ lumps together the effect of inexact hysteresis compensation error and the exogenous disturbance $d_{ex}(t)$. Consequently, closed-loop tracking accuracy is greatly improved if the undesirable perturbation term $d(t)$ could be eliminated using a DOB. Introducing DOB in the feedback system, the analysis in the sequel focuses on the feedback system depicted in Fig. 2. Specifically, the next section studies in detail DOB-based robust disturbance rejection such that the estimate $\hat{d}$ cancels the effect of hysteresis compensation error and exogenous disturbances, in the presence of plant dynamics uncertainty.

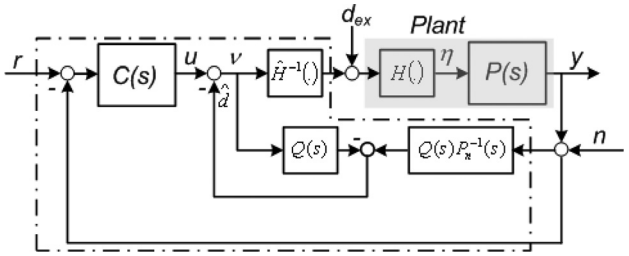

Fig. 2 Inversion-based hysteresis compensation with DOB-based feedback controller (dashed-dot)

4 Robust Disturbance Observers Design

Disturbance observers have been implemented successfully in a wide range of applications including robotic manipulation, high-accuracy hard disk drives servo systems, and machining drive tools (see Refs. [19,21,32,33] and the references therein). Given its importance, synthesis of robust DOBs is an active research topic [20]. In this section, an overview of DOBs is given, robust performance conditions are derived based on closed-loop sensitivity functions, a unified robust design approach for DOBs is developed, and an iterative synthesis algorithm using SDP optimization is presented.

4.1 Overview of Disturbance Observers. From the discussion above, the feedback system in Fig. 2 is redrawn as shown in Fig. 3. In this figure, d collects the effects of hysteresis compensation error and exogenous disturbances. This feedback system is comprised of a two-degree-of-freedom (2-DOF) controller, an internally stabilizing controller $C(s)$ which is assumed to be appropriately designed for nominal tracking performance

$$C(s) = C_c(sI - A_c)^{-1}B_c + D_c \tag{21}$$

and the DOB loop. Within the DOB loop, $Q(s)$ is a stable low pass filter with *unity dc gain and desired bandwidth,* and is considered the design parameter for the DOB.

In Fig. 3, the plant $P(s)$ is represented by the multiplicative uncertainty model [8]

$$P(s) = P_n(s)(1 + \Delta(s)), \quad \Delta(s), \quad ||\Delta||_\infty \le 1, \text{ stable} \tag{22}$$

where $||.||_\infty$ denotes the H_∞ norm [8,27]. $P_n(s)$ represents the nominal plant dynamics, and is given by the state space representation

$$\dot{x}_p = A_p x_p + B_p(\nu + d) \tag{23a}$$

$$y = C_p x_p \tag{23b}$$

where $x_p(t) \in \mathbb{R}^{n_p}$, $y(t) \in \mathbb{R}$, $\nu(t)$, and $d(t)$ are the plant control input and disturbance, respectively. The following assumptions on $P_n(s) = C_p(sI - A_p)^{-1}B_P$ are made

(1) $P_n(s)$ is minimum phase,
(2) A_p is Hurwitz,
(3) The pair (A_p, C_p) is observable.

Assumption 1 implies that the inverse of $P_n(s)$ used in the DOB is stable, together with Assumption 2 are sufficient for internal stability of the DOB-based closed-loop system. Assumption 3 will be used in the DOB design presented in subsequent sections. The primary objective of the DOB is to produce an estimate $\hat{d}$ which is added to the nominal control input u to cancel the effect of d. The *main focus* here is to design $Q(s)$ with desired bandwidth for robust disturbance rejection, which in turn provides robust tracking performance for the overall closed-loop system.

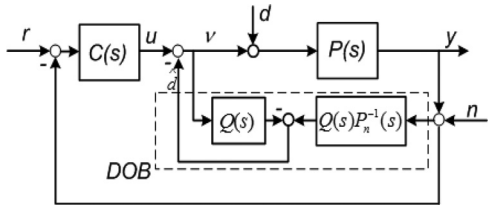

Fig. 3 DOB-based closed-loop system

4.2 Sensitivity Function Analysis. From Fig. 3, assuming that $P_n(s) = P(s)$, the output y is given by

$$y = \frac{P_n(s)C(s)r + P_n(s)(1 - Q(s))d - (P_n(s)C(s) + Q(s))n}{1 + P_n(s)C(s)} \tag{24}$$

The following closed-loop sensitivity functions are defined

$$S(s) = \frac{P_n(s)(1 - Q(s))}{1 + P_n(s)C(s)} \tag{25a}$$

$$T(s) = \frac{P_n(s)C(s) + Q(s)}{1 + P_n(s)C(s)} \tag{25b}$$

From Fig. 3, it is noted that $S(s) = -G_{d\to e}(s)$ is the closed-loop transfer function from $d(t)$ to the tracking $e(t) = r(t) - y(t)$, and $T(s) = -G_{d\to\nu}(s)$ where ν and d define the interconnection variables of the nominal closed-loop and the uncertainty $\Delta(s)$. The expression in Eq. (25*a*) shows that further reduction in $S(s)$ is achieved by having $Q(s) = 1$ over a desired frequency band.

Hence, for a stable weighting function $W_u(s)$ such that $|\Delta(j\omega)| \le |W_u(j\omega)|$ for all ω and for all $\Delta(s)$, it follows that *small gain* condition

$$||W_u T||_\infty < 1 \tag{26}$$

is necessary and sufficient for closed-loop robust stability for the unstructured multiplicative uncertainty (Eq. (22)) [8]. In addition, note that $G_{d\to\hat{d}}(s) = Q(s)$. Thus, given a stable weighting function $W_p(s)$ such that

$$||W_p(1 - Q)||_\infty \le \gamma, \quad \gamma < 1 \Rightarrow ||Wp(d - \hat{d})||_{L_2} \le \gamma||d||_{L_2} \tag{27}$$

where $\gamma > 0$ is a given performance bound and $d - \hat{d}$ is the disturbance estimation error. Consequently, Eqs. (26) and (27) imply that robust disturbance rejection is achieved. In particular, $||W_p(1 - Q)||_\infty \le \gamma$ sets a lower bound on the cut-off frequency of the high pass filter $1 - Q(s)$. Thus, $W_p(s)$ can be selected to reflect desired bandwidth performance constraints on $Q(s)$. The conditions stated in Eqs. (26) and (27) will be used in subsequent sections to formulate a weighted sensitivity optimization for the DOB synthesis.

4.3 Q Filter Design. A typical form of the low pass filter $Q(s)$ used extensively in the literature is [19,21–23,32, 33]

$$Q(s) = \left[1 + \sum_{k=1}^{m-\rho} a_k(\tau s)^k\right]\left[1 + \sum_{k=1}^{m} a_k(\tau s)^k\right]^{-1} \tag{28}$$

where $m > 0$ is the desired order of $Q(s)$ and $\rho \le m$ is its relative degree. The design trade-off of $Q(s)$ is to choose $\{a_k\}_{k=1}^m \ge 0$ such that its cut-off frequency $\omega \approx 1/\tau$ is large enough for better disturbance rejection. However, a direct synthesis of $Q(s)$ in Eq. (28) is subject to

(Q1) *Relative Degree*: ρ must be chosen greater than or equal to that of $P_n(s)$ to enable $Q(s)P_n^{-1}(s)$ to be realizable,

(Q2) *Unity DC gain*: $Q(0) = 1$ imposes that ρ and $\{a_k\}_{k=1}^m$ are not independent of each other [32],

(Q3) Robust stability of the closed-loop system (i.e. Eq. (26)).

These conditions complicate the synthesis of an optimal $Q(s)$. Thus, an alternative design method is desired where the structure constraints (Q1) and (Q2) can be implicitly satisfied to ease the complexity involved. In the next section, the DOB design is formulated as state estimation for an augmented system, which leads to systematic design of $Q(s)$ based on H_∞ weighted-sensitivity optimization.

4.4 DOB Equivalent Observer-Based Disturbance Estimation. In this section, it is shown that under mild conditions, the disturbance estimation based on the DOB is indeed equivalent to the design of a Luenberger observer for an augmented system incorporating an internal model of the disturbance. Once this is established, the DOB filter $Q(s)$ satisfying (Q1), (Q2), and (Q3) can be obtained from the Luenberger observer gain.

Suppose the disturbance d is generated by the autonomous system

$$\dot{x}_d = A_d x_d, \quad d = C_d x_d, \quad x_d(t_0) = x_{d0} \tag{29}$$

where $x_d(t) \in \mathbb{R}^{n_d}$. The following assumptions are made

(4) (A_d, C_d) is detectable,

(5) The eigenvalues of A_d do not coincide with the zeros of the plant $P_n(s)$ (i.e. the disturbance state x_d is observable from the output y).

Let $x = [x_p^T \; x_d^T]^T$, from Eqs. (23) and (29), the augmented state space system is given by

$$\dot{x} = \tilde{A}x + \tilde{B}\nu, \quad \tilde{y} = \tilde{C}x \tag{30a}$$

$$\tilde{A} = \begin{bmatrix} A_p & B_p C_d \\ 0 & A_d \end{bmatrix}, \quad \tilde{B} = \begin{bmatrix} B_p \\ 0 \end{bmatrix}, \quad \tilde{C} = [C_p \quad 0] \tag{30b}$$

Given Assumptions 3, 4, and 5, it can be shown that

$$\operatorname{rank} \begin{bmatrix} \lambda I - A_p & -B_p C_d \\ 0 & \lambda I - A_d \\ C_p & 0 \end{bmatrix} = n_p + n_d \tag{31}$$

for all eigenvalues $\lambda \in \mathbb{C}$ of $\tilde{A}$. Hence it follows from the PBH observability rank condition [27], that the augmented system in Eq. (30) is detectable [20,28]. Thus, there exists $L \in \mathbb{R}^{n_p+n_d}$ such that

$$\dot{\hat{x}} = (\tilde{A} - L\tilde{C})\hat{x} + [\tilde{B} \quad L] \begin{bmatrix} \nu \\ y \end{bmatrix} \tag{32}$$

is an asymptotically stable state observer for the system in Eq. (30). Moreover, using state transformation [20], it can be shown that the eigenvalues of the overall closed-loop system comprised of $P_n(s), C(s)$ and the state observer (Eq. (32)), are given by

$$\det(\lambda I - A_{cl}) = \det \begin{bmatrix} \lambda I - (A_p - B_p D_c C_p) & -B_p C_c \\ B_c C_p & \lambda I - A_c \end{bmatrix} \times \det \begin{bmatrix} \lambda I - (A_p - L_1 C_p) & -B_p C_d \\ L_2 C_p & \lambda I - A_d \end{bmatrix} \tag{33}$$

where $L = [L_1^T \; L_2^T]^T$ with $L_1 \in \mathbb{R}^{n_p}$ and $L_2 \in \mathbb{R}^{n_d}$. This clearly allows a stabilizing controller $C(s)$ to be designed separately of the state estimator. We now consider the following two cases for disturbance estimation:

(1) *Observer-based*: from Eq. (32), the estimate $\hat{d}$ is given by

$$\hat{d} = -G_1(s)\nu + G_2(s)y \tag{34a}$$

where

$$\begin{bmatrix} G_1(s) \\ G_2(s) \end{bmatrix} = \tilde{C}_d (sI - (\tilde{A} - L\tilde{C}))^{-1} \begin{bmatrix} -\tilde{B}, \\ L \end{bmatrix} \tag{34b}$$

where $\tilde{C}_d = [0 \quad C_d]$.

(2) *DOB-based*: from Fig. 3, the estimate $\hat{d}$ is given by

$$\hat{d} = -Q(s)\nu + Q(s)P_n^{-1}(s)y \tag{35}$$

For the synthesis of the low pass filter $Q(s)$ having *unity dc gain*, the following *key assumption* is made:

(6) A_d has at least one of its eigenvalue at the origin.

With the assumptions above, the equivalence between the *DOB-based* estimate in Eq. (35) and the *observer-based* estimate in Eq. (34) is stated next.

Theorem 1. *Given that Assumptions 3, 4, 5, and 6 are satisfied, the expressions in Eqs. (34) and (35) for $\hat{d}$ are equivalent; that is $Q(s) = G_1(s)$ and $Q(s)P_n^{-1}(s) = G_2(s)$. In particular, $Q(0) = G_1(0) = 1$.*

Proof. See pages 543–546 of Ref. [21] for details. □

In particular, the structure constraints (Q1) and (Q2) are satisfied and $Q(s) = G_1(s)$ is a *low-pass filter with unity dc gain*. Thus, once L is obtained, $Q(s)$ is evaluated using $G_1(s)$ in Eq. (34). Specifically, L is desired to be the (sub)optimal solution to the weighted sensitivity H_∞ optimization

$$\min_L \gamma, \quad \text{subject to} : \left\| \begin{bmatrix} W_u T \\ W_p(1-Q) \end{bmatrix} \right\|_\infty \le \gamma, \quad \gamma < 1 \tag{36}$$

The feedback interconnections associated with Eq. (36) is shown in Fig. 4, where the observer transfer function $P_{\text{obs}}(s) = \left[\begin{array}{c|ccc} \tilde{A} & \tilde{B} & 0 & I, \\ \hline \tilde{C}_d & 0 & 0 & 0 \\ -\tilde{C} & 0 & I & 0 \end{array}\right]$, the reference input r, and the measurement noise n are set to zero. The transfer function of the weighted plant $P_W(s)$ is given by

$$P_W(s) = \left[\begin{array}{c|cc} A_W & B_1 & B_2 \\ \hline C_1 & D_{11} & D_{12} \\ C_2 & D_{21} & 0 \end{array}\right] \tag{37}$$

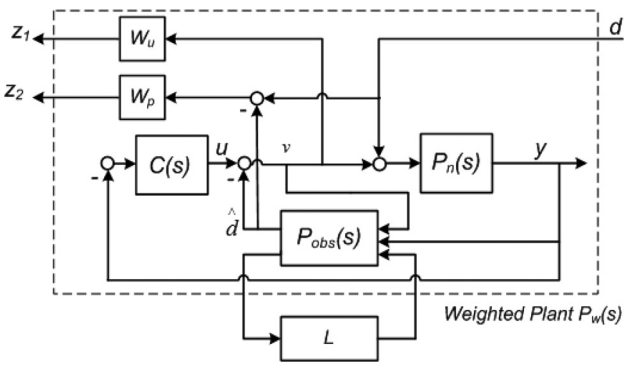

Fig. 4 Weighted plant $P_W(s)$

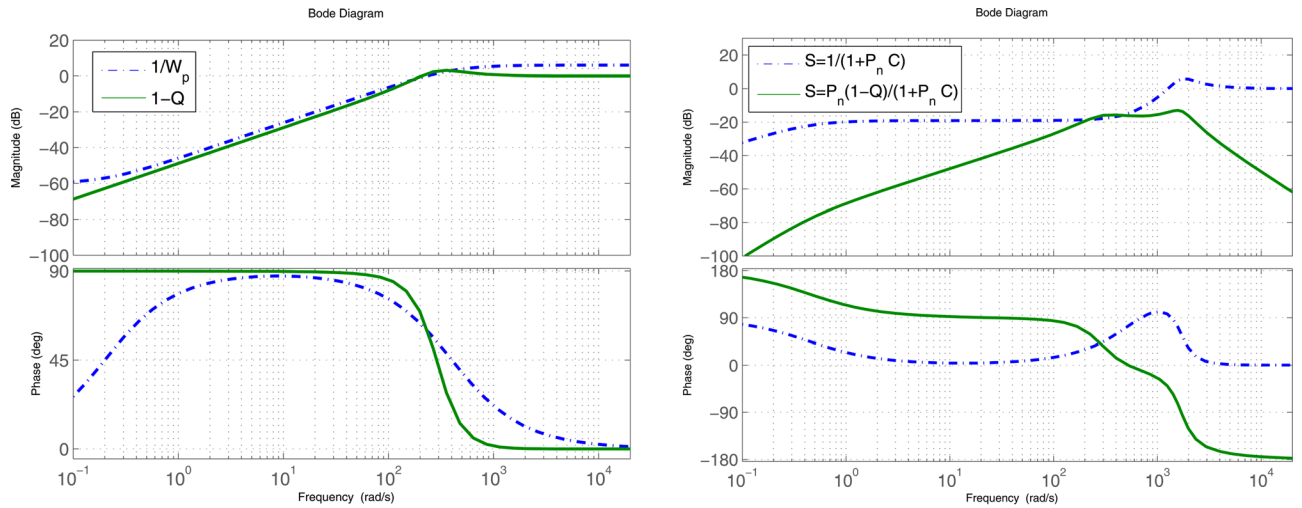

Fig. 5 Bode plots of $1/Wp(s)$ and $1-Q(s)$ (left), closed-loop sensitivity $S(s)$ (right)

Finally, for internally stabilizing $C(s)$, stable $W_u(s)$ and $W_p(s)$, the above discussion states that (A_W, B_2) is stabilizable and (A_W, C_2) is detectable. Hence, assumptions of the standard H_∞ problem are satisfied [27,34,35].

Thus, optimal DOB synthesis is equivalent to robust Luenberger observer satisfying the H_∞ weighted-sensitivity objectives in Eq. (36). This results in an optimization problem over a much simpler structure, namely the static output feedback (SOF) gain of the Luenberger observer, which can be efficiently synthesized using SDP optimization [35,36]. Hence, with proper choice of the weighting functions $W_u(s)$ and $W_p(s)$, robust disturbance rejection is achieved via the optimal synthesis of the Luenberger observer.

Remark. It must be emphasized that the disturbance signal generator in Eq. (29) [24] is only a mathematical tool used in the foregoing analysis of the DOB design, to guarantee *unity DC gain* of $Q(s)$. In particular, the hysteresis compensation error as well as exogenous disturbances in subsequent simulations *are not* generated by Eq. (29).

4.5 The Optimization Task Using Semi-Definite Programming. Given $\gamma > 0$, it follows from the bounded real lemma [27,34], that Eq. (36) is solvable for a stabilizing gain L if and only if there exist positive definite symmetric matrices $P^T = P \succ 0$ and $R^T = R \succ 0$ satisfying

$$\begin{bmatrix} N_1 & 0 \\ 0 & I \end{bmatrix}^T \begin{bmatrix} A_W R + R A_W^T & RC_1^T & B_1 \\ C_1 R & -\gamma I & D_{11} \\ B_1^T & D_{11}^T & -\gamma I \end{bmatrix} \begin{bmatrix} N_1 & 0 \\ 0 & I \end{bmatrix} \prec 0 \quad (38a)$$

$$\begin{bmatrix} N_2 & 0 \\ 0 & I \end{bmatrix}^T \begin{bmatrix} A_W^T P + P A_W & PB_1 & C_1^T \\ B_1^T P & -\gamma I & D_{11}^T \\ C_1 & D_{11} & -\gamma I \end{bmatrix} \begin{bmatrix} N_2 & 0 \\ 0 & I \end{bmatrix} \prec 0 \quad (38b)$$

$$PR = I \quad (38c)$$

where N_1 and N_2 are matrices of the null spaces of $[B_2^T D_{12}^T]$ and $[C_2 D_{21}]$, respectively. The constraints in Eqs. (38*a*), (38*b*), and (38*c*) are not jointly convex in P, R, and γ due to the nonlinear product $PR = I$. This gives rise to computationally intractable bilinear matrix inequality (BMI) constrained SDP optimization [35,36]. One way to solve this nonlinear SDP is to introduce the nonconvex auxiliary cost $J = Trace(PR) + \gamma$, relax the constraint in Eq. (38*c*) into the linear matrix inequality (LMI) $\begin{bmatrix} P & I \\ I & R \end{bmatrix} \succeq 0$, and apply the sequential linear programming matrix algorithm (SLPMM) developed in Ref. [35]. Refer to the Appendix at the end of the paper for details of the SLPMM.

In particular, the SLPMM generates a sequence of linear SDP problems involving the linearization of J, which can be solved very efficiently [25,34]. Once P, R, and γ are determined, the (sub)optimal static gain L is obtained from the feasibility problem

$$\begin{bmatrix} A_W^T P + P A_W & PB_1 & C_1^T \\ B_1^T P & -\gamma I & D_{11}^T \\ C_1 & D_{11} & -\gamma I \end{bmatrix} + \begin{bmatrix} PB_2 \\ 0 \\ D_{12} \end{bmatrix} L \begin{bmatrix} C_2 & D_{21} & 0 \end{bmatrix} + \begin{bmatrix} C_2^T \\ D_{21}^T \\ 0 \end{bmatrix} L^T \begin{bmatrix} B_2^T P & 0 & D_{12}^T \end{bmatrix} \prec 0 \quad (39)$$

5 Robust DOB-Based Hysteresis Compensation: Simulation Results

5.1 Robust DOB Optimization Results. The actuator (plant) dynamics $P(s)$ is given by the lumped parameter system [6,37]

$$y = P(s)(\nu + d) \quad (40)$$

where the output y is the actuator displacement (μm). The plant $P(s)$ and the nominal plant $P_n(s)$ are given by

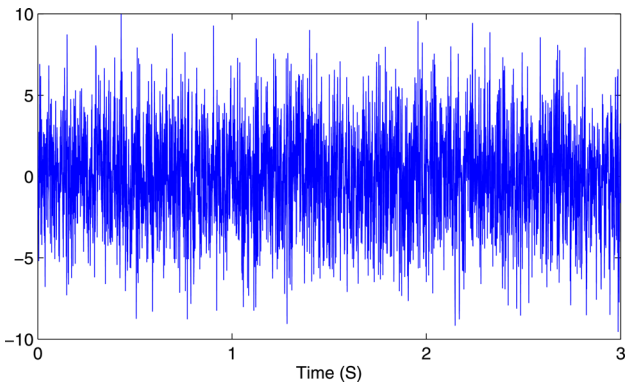

Fig. 6 Sample realization of the external disturbance signal

$$P(s) = \prod_{i=1}^{2} \frac{\omega_i^2}{s^2 + 2\zeta_i \omega_i s + \omega_i^2}, \quad P_n(s) = \frac{\omega_1^2}{s^2 + 2\zeta_1 \omega_1 s + \omega_1^2} \tag{41}$$

where $\zeta_1 = 0.8$ and $\omega_1 = 2\pi(90)$ (rad/s). Note that d represents the hysteresis compensation error and exogenous disturbances. The compensator $C(s)$, designed based on $P_n(s)$, is given by a simple proportional-integral

$$C(s) = 8 + \frac{4}{s} \tag{42}$$

which provides low-frequency high gain for good tracking and nominal robustness. The weighting function $W_p(s)$ is chosen as

$$W_p(s) = 0.5 \frac{s + 2\pi(64)}{s + 0.2} \tag{43}$$

which specifies a cut-off frequency of at least 50 Hz. From Eq. (22), the multiplicative uncertainty weight is given by $W_u(s) = (P(s)/P_n(s)) - 1$. Thus, from the expressions of $P(s)$ and $P_n(s)$, $W_u(s)$ is given by

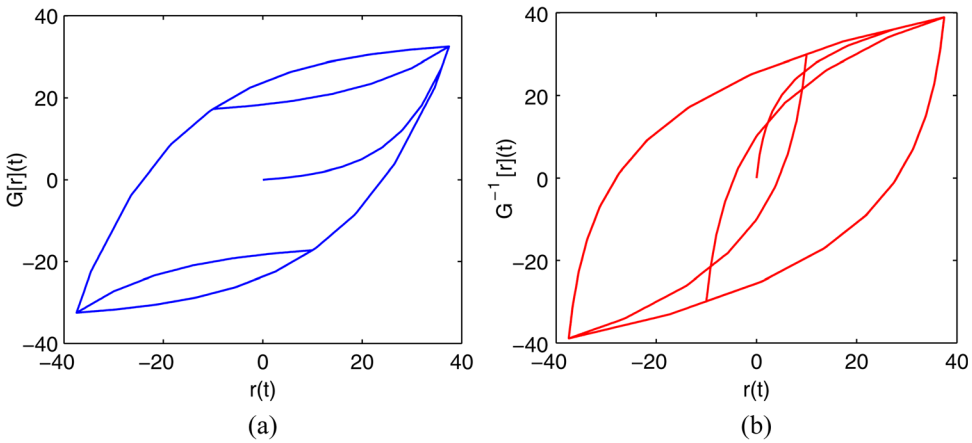

Fig. 7 The input-output relationship between the reference $r(t) = 18\sin(2\pi t) + 28\sin(6\pi t)$ and the output of: (*a*) the Prandtl-Ishlinskii model $G[r](t)$, and (*b*) the inverse Prandtl–Ishlinskii model $G^{-1}[r](t)$

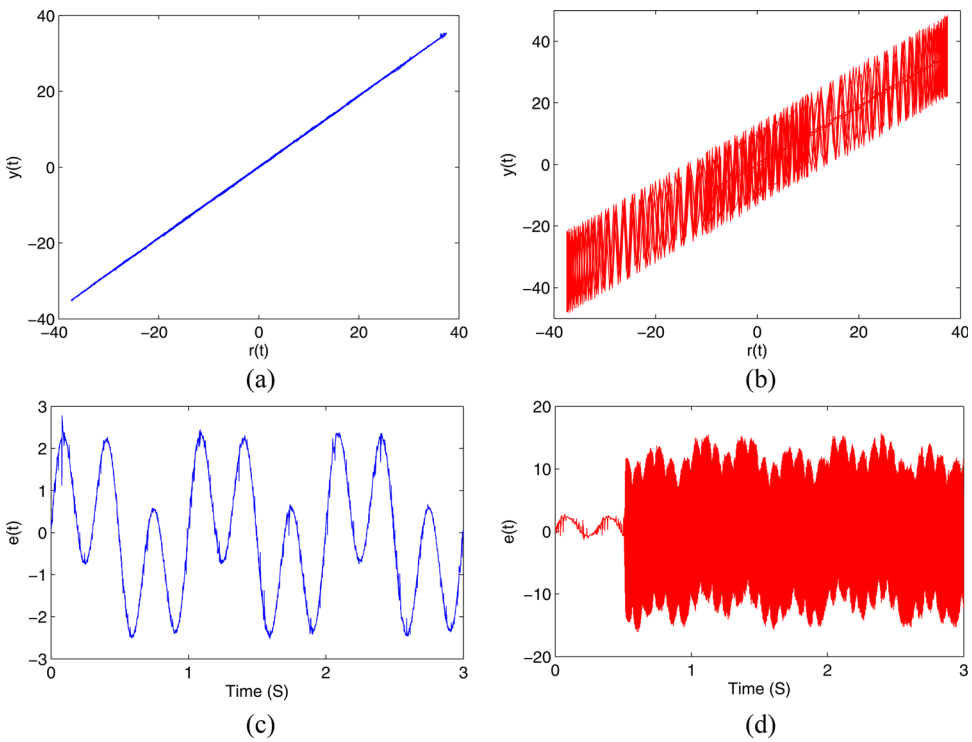

Fig. 8 Example 1: (*a*) and (*b*) show the input-output relationship between the reference input $r(t) = 18\sin(2\pi t) + 28\sin(6\pi t)$ and the output $y(t)$ of the closed-loop system with (*a*) the exact inverse Prandtl–Ishlinskii model $\hat{G}^{-1}[v] = G^{-1}[v]$, and without (*b*) the inverse Prandtl–Ishlinskii model $\hat{G}^{-1}[v] = v$. (*c*) and (*d*) show tracking error $e(t)$ of the closed-loop system for (*a*) and (*b*), respectively.

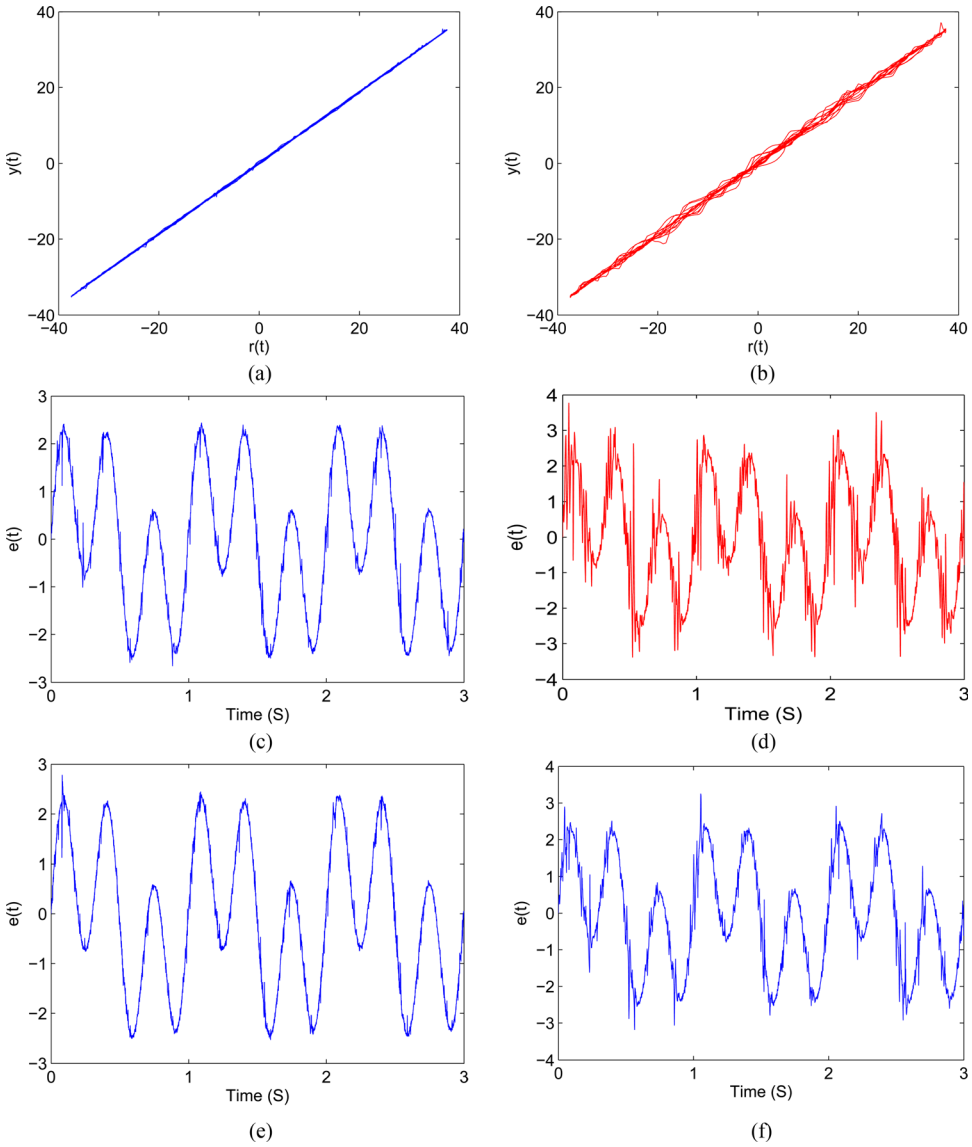

Fig. 9 Example 2: (*a*) and (*b*) show the input-output relationship between the reference input $r(t) = 18\sin(2\pi t) + 28\sin(6\pi t)$ and the output $y(t)$ of the closed-loop system with (*a*) $\hat{G}^{-1} = 0.9G^{-1}$, and (*b*) $\hat{G}^{-1} = 0.5G^{-1}$. (*c*) and (*d*) show the tracking error $e(t)$ of the closed-loop system with (*c*) $\hat{G}^{-1} = 0.9G^{-1}$, and (*d*) $\hat{G}^{-1} = 0.5G^{-1}$. (*e*) and (*f*) show the tracking error $e(t)$ considering $\hat{G}^{-1} = 0.7G^{-1}$ with (*e*) the DOB, and without (*f*) the DOB.

$$W_u(s) = -\frac{s(s + 2\zeta_2\omega_2)}{s^2 + 2\zeta_2\omega_2 s + \omega_2^2} \tag{44}$$

where $\zeta_2 = 0.2$ and $\omega_2 = 2400$ (rad/s). The disturbance model in Eq. (29) is given by the first-order system

$$A_d = 0, \quad C_d = 1 \tag{45}$$

i.e. an integrator $1/s$. This choice implies that $L = \begin{bmatrix} L_1^T & L_2^T \end{bmatrix}^T \in \mathbb{R}^3, L_2 \in \mathbb{R}^2$, and $L_1 \in \mathbb{R}$. Moreover, this simple choice results in the proportional-integral (PI) Luenberger observer structure studied in Ref. [28]

$$\dot{\hat{x}}_p = (A_p - L_1 C_p)\hat{x}_p + B_p C_d \hat{d} + \begin{bmatrix} B_p & L_1 \end{bmatrix} \begin{bmatrix} \nu \\ y \end{bmatrix} \tag{46a}$$

$$\dot{\hat{d}} = -L_2 C_d \hat{x}_p + L_2 y \tag{46b}$$

It can be easily verified that Assumptions 3, 4, 5, and 6 are satisfied. The LMIs in Eqs. (38*a*), (38*b*), and Eq. (A1) are solved using the SEDUMI solver within the YALMIP environment [25], running in MATLAB version 7.9 (R2009b). The optimization is terminated after 14 iterations in 21.512 s resulting in $\gamma = 0.774$ and $L = [-117.381\ 0.197\ 17113.1]^T$. Using Eq. (34*b*), the DOB filter is computed as

$$Q(s) = \frac{5.472 \times 10^9}{s^3 + 6.393 \times 10^4 s^2 + 1.981 \times 10^7 s + 5.472 \times 10^9} \tag{47}$$

which has cut-off frequency at 49 Hz. It is clear from Fig. 5 that $Q(s)$ satisfies the robust performance bound $|1 - Q(j\omega)| \leq |1/W_p(j\omega)| \quad \forall\omega$ (see Eq. (27)), and that the closed-loop sensitivity function $S(s)$ with the DOB (solid) exhibits additional reduction over a wider frequency range than without the DOB (dash-dot).

The closed-loop system with the overall DOB-based feedback systems and the uncertain plant (Eq. (41)), is depicted in Fig. 2. The exogenous disturbance d_{ex} is modeled as a band limited white

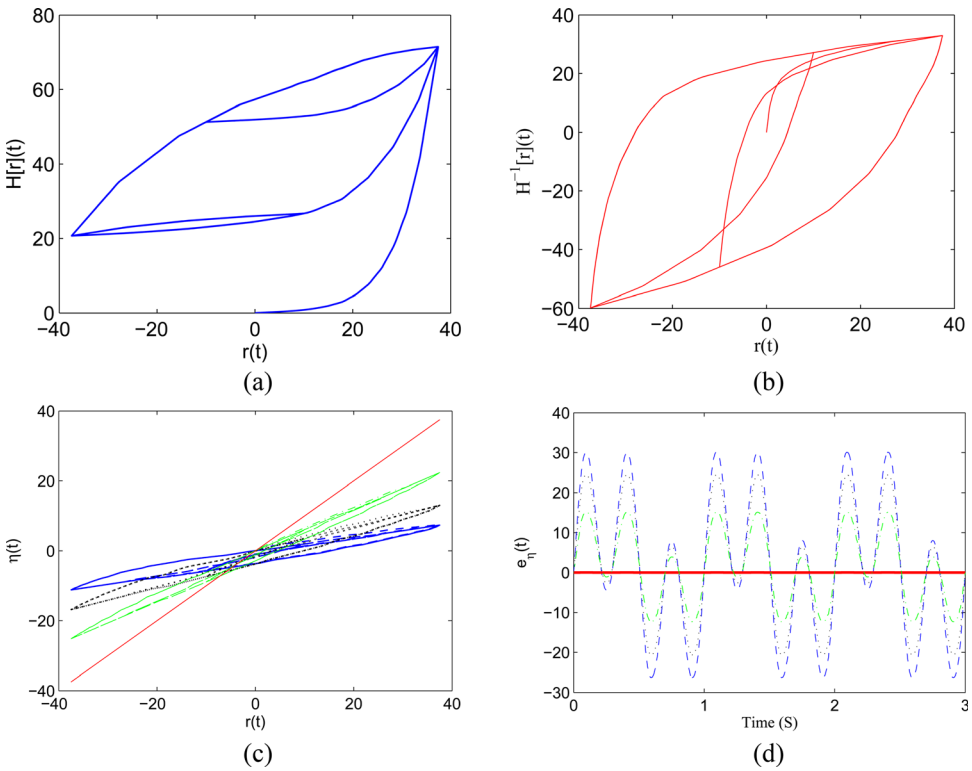

Fig. 10 (*a*) and (*b*) show the input-output relationship between the reference input $r(t) = 18\sin(2\pi t) + 28\sin(6\pi t)$ and (*a*) the output of the generalized Prandtl–Ishlinskii model $H[r](t)$, and (*b*) the output of the inverse generalized Prandtl–Ishlinskii model $H^{-1}[r](t)$. (*c*) shows the input-output relationship between the reference input $r(t)$ and the output of the inverse compensation $H \circ \hat{H}[r](t)$, (*d*) shows the error of the inverse compensation $e_\eta(t) = r(t) - H \circ \hat{H}^{-1}[r](t)$ with $\hat{H}^{-1} = H^{-1}$ (solid line), $\hat{H}^{-1} = 0.9\ H^{-1}$ (dashed-dotted line), $\hat{H}^{-1} = 0.8\ H^{-1}$ (dotted line), and $\hat{H}^{-1} = 0.7\ H^{-1}$ (dashed line).

noise (see Fig. 6). Simulation results are performed for both the Prandtl–Ishlinskii model and its inverse and the generalized Prandtl–Ishlinskii model and its inverse.

5.2 Simulation Results for the Closed-Loop System With the Prandtl–Ishlinskii Model. In this section, the simulation is performed for the closed-loop system in Fig. 2 with the Prandtl–Ishlinskii model G. This model represents a special case of the generalized Prandtl–Ishlinskii model when $\delta(v) = v$, analytically

$$H[v] = G[v] \tag{48}$$

Figure 7 shows the output of the Prandtl–Ishlinskii model $G[r](t)$ and the output of inverse Prandtl–Ishlinskii model $G^{-1}[r](t)$ for the reference input $r(t) = 18\sin(2\pi t) + 28\sin(6\pi t)$. This reference input can show major and minor hysteresis loops when applied as an input for the Prandtl–Ishlinskii model G. We use the following parameters for the Prandtl–Ishlinskii model G: $n = 10$, $r_i = \{4, 8, 12, 16, 20, 24, 28, 32, 36, 40\}$, $g_0 = 0.1, g_i = \{0.0462, 0.069, 0.1029, 0.1535, 0.2291, 0.3417, 0.51, 0.761, 1.1, 1.7,\}$. The parameters of the inverse Prandtl–Ishlinskii model G^{-1} computed using Eqs. (7) and (8) are: $s_i = \{0.4,\ 0.985,\ 1.8459,\ 3.1186,\ 5.00,\ 7.8085,\ 11.9784,\ 18.1875,\ 27.4386,\ 41.2279\}$, $\hat{g}_0 = 10$, $\hat{g}_i = \{-3.16, -2.1918,\ -1.5030,\ -1.0231,\ -0.6930,\ -0.4678,\ -0.315,\ -0.2118,\ -0.1423,\ -0.0955\}$. A number of studies proposed linear controllers to compensate for the error of the inverse compensation when the estimated inverse hysteresis model is applied as a feedforward compensator (i.e. open-loop inverse-based); see, e.g., Ref. [38]. In this study, the controller $C(s)$ is given by Eq. (42). The simulation results show significant improvement in hysteresis compensation and tracking error $e(t) = r(t) - y(t)$ when the inverse-based scheme and the DOB are both employed.

5.2.1 Example 1. In this example, we consider the closed-loop system in Fig. 2 with and without the exact inverse Prandtl–Ishlinskii model. Figure 8 shows simulation results for the output $y(t)$ with and without the exact inverse of the Prandtl–Ishlinskii model. The results show that the Prandtl–Ishlinskii model $\hat{G}^{-1}[v] = G^{-1}[v]$ yields linear input-output relationship between the reference input $r(t) = 18\sin(2\pi t) + 28\sin(6\pi t)$ and the output $y(t)$, while the output $y(t)$ without the inverse Prandtl–Ishlinskii model $\hat{G}^{-1}[v] = v$ shows high oscillations. The figure shows high tracking error $e(t) = r(t) - y(t)$ with undesirable high limit cycle oscillations in the absence of the inverse Prandtl–Ishlinskii model $\hat{G}^{-1}[v] = v$.

5.2.2 Example 2. This example refers to the overall closed-loop system in Fig. 2. In this example, we consider $\hat{G}^{-1} = 0.9\ G^{-1}$ and $\hat{G}^{-1} = 0.5\ G^{-1}$. Figure 9 shows better performance for the closed-loop system with the estimated inverse Prandtl–Ishlinskii model $\hat{G}^{-1} = 0.9\ G^{-1}$. Figure 9(*e*) and Fig. 9(*f*) show the tracking error $e(t)$ with and without the DOB, when the estimated inverse Prandtl–Ishlinskii model $\hat{G}^{-1} = 0.7\ G^{-1}$ is applied. The results show 50% improvement in the tracking error performance of the closed-loop system. It is obvious that the tracking error in Fig. 9(*f*) is comparable to that of exact hysteresis compensation in Fig. 8(*c*).

5.3 Simulation Results for the Closed-Loop System With the generalized Prandtl–Ishlinskii Model. In this section, we present simulation results for the closed-loop system in Fig. 2 with the generalized Prandtl–Ishlinskii model H and its estimated

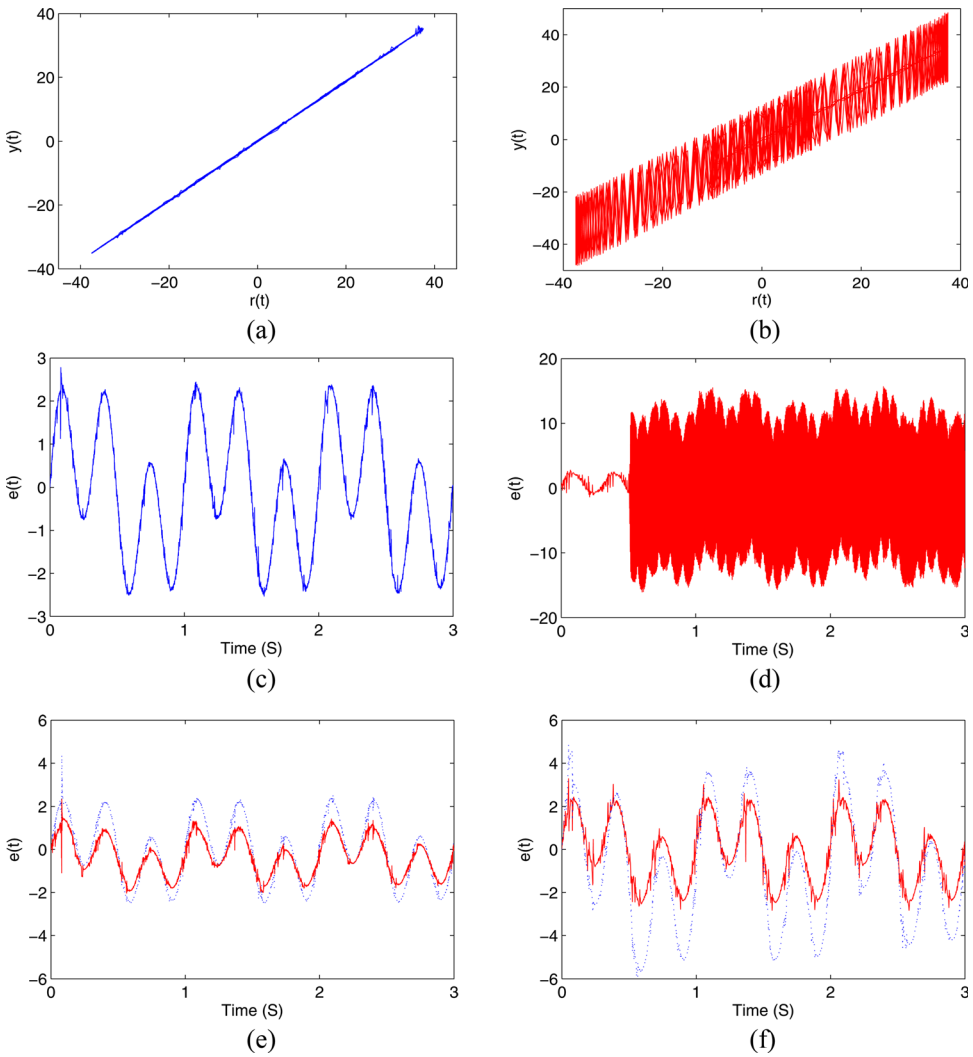

Fig. 11 Example 3. (*a*) and (*b*) show the input-output relationship between the reference input $r(t) = 18\sin(2\pi t) + 28\sin(6\pi t)$ and the output of the closed-loop system $y(t)$ with the DOB and with (*a*) the exact inverse generalized Prandtl–Ishlinskii model $\hat{H}^{-1}[v] = H^{-1}[v]$, and without (*b*) the inverse generalized Prandtl–Ishlinskii model $\hat{H}^{-1}[v] = v$. (*c*) and (*d*) the tracking error $e(t)$ of the closed-loop system of (*a*) and (*b*), respectively. (*e*) and (*f*) show the tracking error $e(t)$ of the closed-loop system with the DOB (solid line) and without the DOB (dashed line) with (*e*) $\hat{H}^{-1} = 0.95\ H^{-1}$, and with (*f*) $\hat{H}^{-1} = 0.7\ H^{-1}$.

inverse $\hat{H}^{-1}$. We use the Prandtl–Ishlinskii model G in the previous subsection and the following function δ

$$\delta(v) = \Gamma[v] = \sum_{i=0}^{m} \xi_i S_{\rho_i}(v) \tag{49}$$

where

$$S_{\rho_i}(v) = \max(v - \rho_i, 0) \tag{50}$$

g_i are constants, and ρ_i are thresholds such that

$$0 = \rho_0 \le \rho_1 \le \cdots \le \rho_m \tag{51}$$

The inverse memoryless model is expressed as

$$\Gamma^{-1}(v) = \sum_{i=0}^{m} \varepsilon_i S_{\psi_i}(v) \tag{52}$$

where

$$\psi_i = \sum_{j=0}^{i} \xi_j(\rho_i - \rho_j) \tag{53}$$

$$\varepsilon_0 = \frac{1}{\xi_0} \tag{54}$$

and

$$\varepsilon_i = \frac{-\xi_i}{\left(\xi_0 + \sum_{j=1}^{i} \xi_j\right)\left(\xi_0 + \sum_{j=1}^{i-1} \xi_j\right)} \tag{55}$$

We use the following parameters for the memoryless model Γ: $m = 3$, $\xi_0 = 0.65, \xi_1 = 0.2, \xi_2 = 0.3, \xi_3 = 0.4, \rho_1 = 7.56, \rho_2 = 12$, $\rho_3 = 17.69$. The parameters of the inverse memoryless model Γ^{-1} computed using Eqs. (54) and (55) are $\psi_1 = 4.94$, $\psi_2 = 8.688, \psi_3 = 15.2315, \varepsilon_0 = 1.5385, \varepsilon_1 = -0.361, \varepsilon_2 = -0.3069$, and $\varepsilon_3 = -0.2244$. We use the reference input $r(t) = 18\sin(2\pi t)$

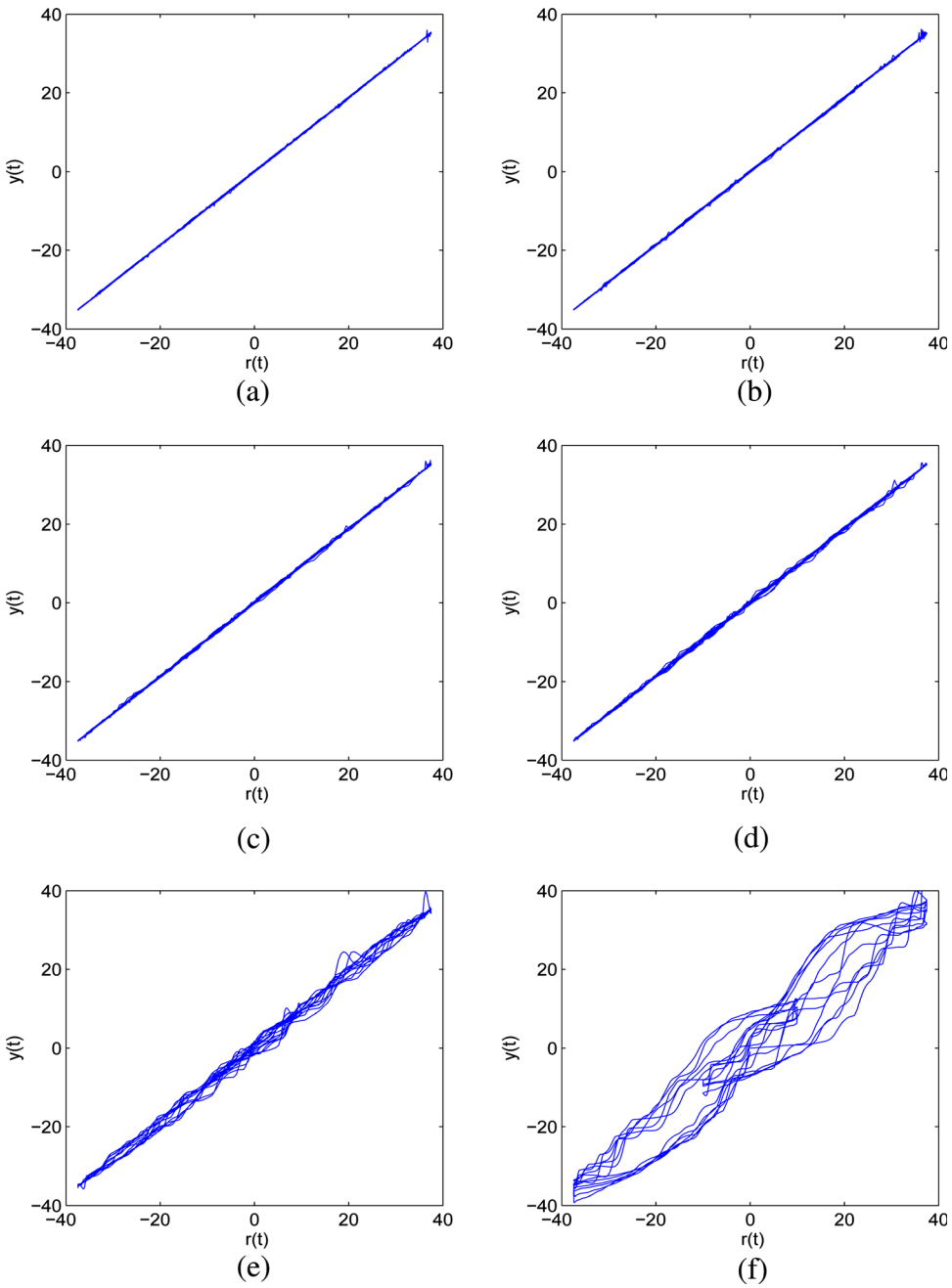

Fig. 12 Example 4. The input-output relationship between the reference input $r(t) = 18\sin(2\pi t) + 28\sin(6\pi t)$ and the output of the closed-loop system $y(t)$ with (*a*) $\hat{H}^{-1} = H^{-1}$, (*b*) $\hat{H}^{-1} = 0.9\ H^{-1}$, (*c*) $\hat{H}^{-1} = 0.8\ H^{-1}$, (*d*) $\hat{H}^{-1} = 0.7\ H^{-1}$, (*e*) $\hat{H}^{-1} = 0.4\ H^{-1}$, and (*f*) $\hat{H}^{-1} = 0.1\ H^{-1}$.

$+28\sin(6\pi t)$. The output of the generalized Prandtl–Ishlinskii model $H[r](t)$ and its inverse $\hat{H}^{-1}[r](t)$ are shown in Figs. 10(*a*) and 10(*b*). The output of the inverse compensation $H \circ \hat{H}^{-1}[r](t)$ when the estimated inverse generalized Prandtl–Ishlinskii model $\hat{H}^{-1}[r](t)$ is applied as a feedforward compensator to compensate for the hysteresis nonlinearities of the generalized Prandtl–-Ishlinskii model $H[r](t)$ is shown in Fig. 10(*c*). The figure shows hysteresis nonlinearity between the reference input $r(t)$ and the output of the compensation $H \circ \hat{H}^{-1}[r](t)$. Figure 10(*d*) shows the time history of the compensation error $e_\eta(t) = r(t) - H \circ \hat{H}^{-1}[r](t)$.

5.3.1 Example 3. This example refers to the overall closed-loop system in Fig. 2. Figures 11(*a*)–11(*d*) show the output of the closed-loop system $y(t)$ and the tracking error $e(t)$ with and without the exact inverse generalized Prandtl–Ishlinskii model. The tracking error $e(t)$ of the closed-loop system with the estimated inverse generalized Prandtl– Ishlinskii model $\hat{H}^{-1} = 0.95\ H^{-1}$ and $\hat{H}^{-1} = 0.7\ H^{-1}$ with and without the DOB are shown in Fig. 11(*e*) and Fig. 11(*f*), respectively.

5.3.2 Example 4. This example refers to the overall closed-loop system in Fig. 2. Figure 12 shows the input-output relationship between the reference $r(t)$ and the output of the closed-loop system $y(t)$ with the estimated inverse generalized Prandtl–Ishlinskii model of $\hat{H}^{-1} = H^{-1}, \hat{H}^{-1} = 0.9\ H^{-1}, \hat{H}^{-1} = 0.8\ H^{-1}$, $\hat{H}^{-1} = 0.7\ H^{-1}, \hat{H}^{-1} = 0.4\ H^{-1}$, and $\hat{H}^{-1} = 0.1\ H^{-1}$.

6 Conclusions

This paper studied performance enhancement for inverse-based hysteresis compensation using disturbance observers to account for exogenous disturbances and inexact hysteresis compensation. The approach presented brings together established hysteresis compensation techniques and tools from robust control theory, leading to guaranteed robust closed-loop performance. Moreover, simulation results indicate that the closed-loop system, with the combined inverse-based compensation and the DOB, shows better performance than the feedforward inverse-based approach which suffers from potential limit-cycle oscillations.

Acknowledgment

This work was supported by the Czech Science Foundation Grant No. P201/2010/2315 and by RVO: 67985840.

Appendix: SLPMM Algorithm

The SLPMM algorithm is given the following iterations:

(1) Solve the initialization feasibility problem: Find $P_0 \succ 0$, $R_0 \succ 0$ and $\gamma_0 > 0$ which satisfy Eqs. (38*a*) and (38*b*), and the SDP relaxation

$$\begin{bmatrix} P & I \\ I & R \end{bmatrix} \succeq 0 \tag{A1}$$

(2) For $k = 0,1,2,\ldots$, solve

$$\min_{P\succ 0, R\succ 0, \gamma>0} J_L := Trace(PR_k + P_k R) + \gamma \tag{A2}$$

subject to: $\gamma < 1$, Eqs. (38*a*), (38*b*), and (A1),

(3) Set $\delta P_k = P - P_k, \delta R_k = R - R_k$ and $\delta\gamma_k = \gamma - \gamma_k$. Compute

$$\alpha_k = \underset{0\le\alpha\le 1}{\operatorname{argmin}} \left(Trace[(P_k + \alpha\delta P_k)(R_k + \alpha\delta R_k)] + \gamma_k + \alpha\delta\gamma_k\right) \tag{A3}$$

(4) Set $P_{k+1} = P_k + \alpha_k\delta P_k, R_{k+1} = R_k + \alpha_k\delta R_k$ and $\gamma_{k+1} = \gamma_k + \alpha_k\delta\gamma_k$.

(5) If a termination condition is satisfied, stop. Otherwise, go to step 2.

The line search in Eq. (A3) computes the step size $\alpha \in [01]$ to ensure successive reduction in the value of J_L[1]. It is shown in Ref. [35] that for a nonempty constraint set, the SLPMM generates strictly decreasing bounded sequences $\{P_k\}, \{R_k\}$, and $\{\gamma_k\}$ which converge to a (sub) optimal solution lying in the boundary of the constraint set, i.e., $PR = I$. For more details refer to Ref. [35] and the references therein.

References

[1] Smith, R. C., 2005, *Smart Material Systems: Model Development*, Society for Industrial and Applied Mathematics, Philidelphia, PA.

[2] Al Janaideh, M., and Krejčí, P., 2012, "Inverse Rate-Dependent Prandtl-Ishlinskii Model for Feedforward Compensation of Hysteresis in a Piezomicropositioning Actuator," IEEE/ASME Trans. Mechatron., **PP**(99), pp 1–10.

[3] Esbrook, A., Guibord, M., Tan, X., and Khalil, H., 2010, "Control of Systems With Hysteresis via Servocompensation and its Application to Nanopositioning," Proceedings of the American Control Conference, Baltimore, MD, pp. 6531–6536.

[4] Krejčí, P., Al Janaideh, M., and Deasy, F., 2012, "Inversion of Hysteresis and Creep Operators," Phys. B, **407**(9), pp. 1354–1356.

[5] Al Janaideh, M., and Krejčí, P., 2011, "An Inversion Formula for a Prandtl-Ishlinskii Operator with Time-Dependent Thresholds," Phys. B, **406**(8), pp. 1528–1532.

[6] Tan, X., and Khalil, H., 2007, "Control Unknown Dynamic Hysteretic Systems Using Slow Adaption: Preliminary Results," Proceedings of the American Control Conference, New York, pp. 3294–3299.

[7] Krejčí, P., and Kuhnen, K., 2001, "Inverse Control of Systems With Hysteresis and Creep," IEEE Proc. Control Theory Appl., **148**(3), pp. 185–192.

[8] Doyle, J., Francis, B., and Tannenbaum, A., 1990, *Feedback Control Theory*, Macmillan Publishing Co., New York.

[9] Al Janaideh, M., and Krejčí, P., 2012, "Prandtl-Ishlinskii Hysteresis Models for Complex Time Dependent Hysteresis Nonlinearities," Phys. B, **407**(9), pp. 1365–1367.

[10] Davino, D., Natale, C., Pirozzi, S., and Visone, C., 2004, "A Phenomenological Dynamic Model of a Magnetostrictive Actuator," Phys. B, **343**(1–4), pp. 112–116.

[11] Al Janaideh, M., Yan, J., D'Amato, A., and Bernstein, D., 2012, "Retrospective-Cost Adaptive Control of Uncertain Hammerstein-Wiener Systems with Memoryless and Hysteretic Nonlinearities," Proceedings of AIAA Guidance, Navigation, and Control Conference, Minneapolis, MN, Paper No. AIAA-2012-4449-671, pp. 1–26.

[12] Al Janaideh, M., Sumer, E., Yan, J., Anthony, D., Drincic, B., Aljanaideh, K., and Bernstein, D., 2012, "Adaptive Control of Uncertain Linear Systems With Uncertain Hysteretic Input Nonlinearities," Proceedings of the 5th Annual Dynamic Systems and Control Conference, Ft. Lauderdale, FL, pp. 1–10.

[13] Nealis, J., and Smith, R. C., 2007, "Model-Based Robust Control Design for Magnetostrictive Transducers Operating in Hysteretic and Nonlinear Regimes," IEEE Trans. Control Syst. Technol., **15**(1), pp. 22–39.

[14] Al Janaideh, M., Feng, Y., Rakheja, S., Tan, Y., and Su, C.-Y., 2009, "Generalized Prandtl-Ishlinskii Hysteresis: Modeling and Robust Control," Proceedings of the IEEE Conference on Decision and Control, Shanghai, China, pp. 7279–7284.

[15] Al Janaideh, M., Rakheja, S., and Su, C.-Y., 2009, "Experimental Characterization and Modeling of Rate-Dependent Hysteresis of a Piezoceramic Actuator," Mechatronics, **19**(5), pp. 656–670.

[16] Visone, C., and Sjöström, M., 2004, "Exact Invertible Hysteresis Models Based on Play Operators," Phys. B, **343**, pp. 148–152.

[17] Al Janaideh, M., Rakheja, S., and Su, C.-Y., 2011, "An Analytical Generalized Prandtl-Ishlinskii Model Inversion for Hysteresis Compensation in Micro Positioning Control," IEEE/ASME Trans. Mechatron., **16**(4), pp. 734–744.

[18] Kuhnen, K., 2003, "Modeling, Identification and Compensation of Complex Hysteretic Nonlinearities-A Modified Plandtl-Ishlinskii Approach," Eur. J. Control, **9**(4), pp. 407–418.

[19] Bickel, R., and Tomizuka, M., 1999, "Passivity-Based Versus Disturbance Observer Based Robot Control: Equivalence and Stability," J. Dyn. Syst., Meas. Control, **121**(1), pp. 41–47.

[20] El-Shaer, A. H., Zhang, T., and Al Janaideh, M., 2011, "On Robust Distrubance Observer Design Using Semi-Definite Programming," Proceedings of the Dynamic Systems Control Conference, Arlington, VA, pp. 1–7.

[21] Schrijver, E., and Dijk, J. V., 2002, "Disturbance Observers for Rigid Mechanical Systems: Equivalence," Stab. Des., J. Dyn. Syst., Meas. Control, **124**(4), pp. 539–548.

[22] Shahruz, S. M., 2000, "Performance Enhancement of a Class of Nonlinear Systems by Disturbance Observers," IEEE/ASME Trans. Mechatron., **5**(3), pp. 319–323.

[23] Wang, C. C., and Tomizuka, M., 2004, "Design of Robustly Stable Disturbance Observers Based on Closed Loop Consideration Using H_∞ Optimization and its Applications to Motion Control," Proceedings of the American Control Conference, Boston, MA, pp. 3764–3769.

[24] Johnson, C. D., 1971, "Accommodation of External Disturbances in Linear Regulator and Servomechanism Problems," IEEE Trans. Autom. Control, **16**(6), pp. 635–644.

[25] Lofberg, J., 2010, "YALMIP," http://control.ee.ethz.ch/joloef/yalmip.php

[26] Mita, T., Hirata, M., Murata, K., and Zhang, H., 1998, "H_∞ Control Versus Disturbance-Observer-Based Control," IEEE Trans. Ind. Electron., **45**(3), pp. 488–495.

[27] Dullerud, G. E., and Paganini, F., 2000, *A Course in Robust Control Theory*, Springer-Verlag, New York.

[28] Söffker, D., Yu, T., and Müller, P. C., 1995, "State Estimation of Dynamical Systems With Nonlinearities by Using Proportional-Integral Observer," Int. J. Syst. Sci., **26**(9), 1571–1582.

[29] Al Janaideh, M., 2009, "Generalized Prandtl-Ishlinskii Hysteresis Model and its Analytical Inverse for Compensation of Hysteresis in Smart Actuators," Ph.D. thesis, Concordia University, Montreal, Canada.

[30] Cao, C., and Hovakimyan, N., 2006, "Design and Analysis of a Novel L1 Adaptive Control Architecture with Guaranteed Transient Performance," Proceedings of the American Control Conference, Minneapolis, MN, pp. 3397–3402.

[31] Fan, X., and Smith, R., 2008, "Model-Based L1 Adaptive Control of Hysteresis in Smart Materials," Proceedings of the IEEE Conference on Decision and Control, Cancun, Mexico, pp. 3251–3256.

[32] Umeno, T., Kaneko, T., and Hori, Y., 1993, "Robust Servosystem Design with Two Degrees of Freedom and its Application to Novel Motion Control of Robot Manipulators," IEEE Trans. Ind. Electron., **40**(5), pp. 473–485.

[1]The command fmincon in MATLAB is used to compute α in Eq. (A3).

[33] Kim, B. K., and Chung, W. K., 2003, "Advanced Disturbance Observer Design for Mechanical Positioning Systems," IEEE Trans. Ind. Electron., **50**(6), pp. 1207–1216.
[34] Gahinet, P., and Apkarian, P., 1994, "A Linear Matrix Inequality Approach to H_∞ Control," Int. J. Robust Nonlinear Control, **4**(4), pp. 421–448.
[35] Leibfritz, F., 2001, "An LMI-Base Algorithm for Designing Suboptimal Static H_2/H_∞ Output Feedback Controllers," SIAM J. Control Optim., **39**(6), pp. 1711–1735.
[36] L. El Ghaoui, F. Oustry, and M. AitRami, 1997, "A Cone Complementarity Linearization Algorithm for Static Output-Feedback and Related Problems," *IEEE Transactions on Automatic Control*, **42**(8), pp. 1171–1176.
[37] Al Janaideh, M., Feng, Y., Rakheja, S., Su, C.-Y., and Rabbath, C., 2009, "Hysteresis Compensation for Smart Actuators Using Inverse Generalized Prandtl-Ishlinskii Model," Proceedings of the American Control Conference, St. Louis, MO, pp. 307–312.
[38] Ge, P., and Jouaneh, M., 1996, "Tracking Control of a Piezoceramic Actuator," IEEE Trans. Control Syst. Technol., **4**(3), pp. 209–216.